

Particle-resolved
modeling of a ship
plume

J. Tian et al.

Modeling the evolution of aerosol particles in a ship plume using PartMC-MOSAIC

J. Tian¹, N. Riemer¹, L. Pfaffenberger², H. Schlager³, and A. Petzold⁴

¹Department of Atmospheric Sciences, University of Illinois at Urbana-Champaign, Urbana, Illinois, USA

²Laboratory of Atmospheric Chemistry, Paul Scherrer Institute, 5232 Villigen, Switzerland

³Dt. Zentrum für Luft- und Raumfahrt, Inst. für Physik der Atmosphäre, Oberpfaffenhofen, 82234 Wessling, Germany

⁴Forschungszentrum Jülich GmbH, Institute of Energy and Climate Research, Jülich, Germany

Received: 6 May 2013 – Accepted: 7 June 2013 – Published: 21 June 2013

Correspondence to: N. Riemer (nriemer@illinois.edu)

Published by Copernicus Publications on behalf of the European Geosciences Union.

Title Page

Abstract

Introduction

Conclusions

References

Tables

Figures

⏪

⏩

◀

▶

Back

Close

Full Screen / Esc

Printer-friendly Version

Interactive Discussion



Abstract

This study investigates the evolution of ship-emitted aerosol particles using the stochastic particle-resolved model PartMC-MOSAIC. Comparisons of our results with observations from the QUANTIFY Study in 2007 in the English channel and the Gulf of Biscay showed that the model was able to reproduce the observed evolution of total number concentration and the vanishing of the nucleation mode consisting of sulfate particles. Further process analysis revealed that during the first hour after emission, dilution reduced the total number concentration by four orders of magnitude, while coagulation reduced it by an additional order of magnitude. Neglecting coagulation resulted in an overprediction of more than one order of magnitude in the number concentration of particles smaller than 40 nm at a plume age of 100 s. Coagulation also significantly altered the mixing state of the particles, leading to a continuum of internal mixtures of sulfate and black carbon. The impact on cloud condensation nuclei (CCN) concentrations depended on the supersaturation threshold S at which CCN activity was evaluated. For the base case conditions simulated here, characterized by a low formation rate of secondary aerosol species, neglecting coagulation led to an underestimation of CCN concentrations of about 20 % for $S = 0.6 %$ and of about 40 % for $S = 0.3 %$. For $S = 0.1 %$ the differences between simulations including coagulation and neglecting coagulation were negligible.

1 Introduction

Emissions from ocean-going ships have been receiving increased attention in recent years due to their adverse effects on coastal and global air quality (Ault et al., 2009; Endresen et al., 2003; González et al., 2011; Moldanová et al., 2009; Eyring et al., 2007), human health (Corbett et al., 2007; Winebrake et al., 2009) and the climate system (Capaldo et al., 1999; Eyring et al., 2010; Lawrence and Crutzen, 1999). Aerosol particles from ship exhaust represent a large fraction of global anthropogenic aerosol

Particle-resolved modeling of a ship plume

J. Tian et al.

Title Page

Abstract

Introduction

Conclusions

References

Tables

Figures



Back

Close

Full Screen / Esc

Printer-friendly Version

Interactive Discussion



emissions (Agrawal et al., 2009; Dominguez et al., 2008) and influence significantly the radiative budget of the atmosphere both directly and indirectly (Capaldo et al., 1999).

Ship-emitted particulates are a mix of different particle types. These include combustion particles consisting mainly of black carbon (BC), primary organic carbon (POC), sulfate and ash, and volatile particles forming from nucleation of sulfuric acid during plume expansion (Song et al., 2003; Cooper, 2003; Petzold et al., 2008). Their overall direct effect on the climate system is complex since BC causes a positive radiative forcing, while sulfuric acid particles cause a negative radiative forcing (Lauer et al., 2007; Kasper et al., 2007). While the different particle types are initially externally mixed, internal mixtures can form as a result of coagulation and condensation processes as the plume evolves, which may significantly alter the particles' optical properties and hence the magnitude of the direct climate impact (Durkee et al., 2000b; Jacobson et al., 2011). Particles from ship exhaust can also act as cloud condensation nuclei (CCN) and thus indirectly affect the climate by increasing cloud reflectivity (Twomey et al., 1968; Durkee et al., 2000b,a; Porph et al., 1999; Russell et al., 2000; Peters et al., 2012). The "ship tracks", shown as the curvilinear cloud structures observed in satellite images of marine cloud fields, in fact represented the first evidence of an indirect effect by ship emissions (Conover, 1966; Coakley et al., 1987). Similar to the particles' optical properties, their CCN properties may change during the plume evolution, which in turn impacts their indirect effect.

Many studies have been conducted in the past decade to characterize the ship emissions and their effects on climate through a combination of exhaust and plume measurements (Murphy et al., 2009; Frick and Hoppel, 2000; Petzold et al., 2008; Osborne et al., 2001; Sinha et al., 2003; Coggon et al., 2012). To quantify the in-plume mixing state Ault et al. (2010) conducted a series of individual ship plume measurements at the port of Los Angeles using a 4 m sampling mast at a site near the center of the main channel. The measurements characterized the size-resolved particle mixing state for individual plumes with plume ages ranging between 10–45 min. Their study showed

Particle-resolved modeling of a ship plume

J. Tian et al.

Title Page

Abstract

Introduction

Conclusions

References

Tables

Figures



Back

Close

Full Screen / Esc

Printer-friendly Version

Interactive Discussion



enhanced sulfate concentration in ship plumes, probably due to vanadium-catalyzed sulfate-production reactions in the plume within minutes of emission.

The evolution of ship-emitted particles has also been investigated in a number of modeling studies. Russell et al. (1999) applied an externally mixed, sectional aerosol dynamic model to characterize condensational and coagulative particle growth during the Monterey Area Ship Tracks (MAST) experiment in 1994 and found that the sulfur content of fuels used in combustion processes had a direct impact on the CCN properties. Later Erlick et al. (2001) applied the same model as described in Russell et al. (1999) together with a delta-Eddington exponential-sum-fit radiation algorithm to simulate aerosol-cloud-interaction during two ship track events in the MAST experiment. The results suggested that both the marine clouds and ship tracks enhanced atmospheric absorption with respect to a clear sky. Song et al. (2003) used a Lagrangian photochemical plume model to explore the in-plume sulfur chemistry and new particle formation. Their findings stressed the importance of photochemistry for the production of sulfuric acid particles in plumes. von Glasow et al. (2003) introduced a plume expansion scheme in a time dependent photochemical model based on an updated version of the box model MOCCA (Model Of Chemistry Considering Aerosols) (Sander and Crutzen, 1996; Vogt et al., 1996) to treat the mixing of background and plume air. The evolution of particles in the plume was tracked by considering dilution and chemical processes, while coagulation was neglected. The influence of semi-volatile background aerosol particles was found to be important for the in-plume gas phase chemistry, while including the soluble ship-produced aerosols was of little importance for in-plume heterogeneous reactions since dilution significantly reduced ship-derived particles on a very short time scale.

For this study we used a new modeling approach to represent the evolving particle distribution of ship-emitted aerosols, the stochastic particle-resolved aerosol model PartMC-MOSAIC (Particle Monte Carlo model-Model for Simulating Aerosol Interactions and Chemistry) (Riemer et al., 2009). This model explicitly resolves the composition of individual particles in a given aerosol population and is therefore uniquely suited

Particle-resolved modeling of a ship plume

J. Tian et al.

Title Page

Abstract

Introduction

Conclusions

References

Tables

Figures

◀

▶

◀

▶

Back

Close

Full Screen / Esc

Printer-friendly Version

Interactive Discussion



Particle-resolved modeling of a ship plume

J. Tian et al.

Title Page

Abstract

Introduction

Conclusions

References

Tables

Figures

◀

▶

◀

▶

Back

Close

Full Screen / Esc

Printer-friendly Version

Interactive Discussion



to investigate the evolution of particle mixing states and the associated particle properties. The simulations were initialized with gas and particle information obtained from a test-rig study as part of the European research project HERCULES (High-efficiency Engine R&D on Combustion with Ultra-Low Emissions for Ships) in 2006 using a serial
5 four-stroke marine diesel engine operating on high-sulfur heavy fuel oil (Petzold et al., 2008). We then tracked the particle population for several hours as it evolved undergoing coagulation, dilution with the background air, and chemical transformations in the aerosol and gas phase. We compared the results to aircraft measurements made in the English Channel and the Gulf of Biscay (France) in 2007 as part of the European program QUANTIFY (Quantifying the Climate Impact of Global and European Transport Systems) (Pfaffenberger et al., 2013).
10

The scientific contribution of this study is twofold. First, it is the first process study on the evolution of the particle-resolved mixing state in ship plumes quantifying the roles of coagulation and condensation in the plume and their impact on CCN properties
15 of the particles. Second, this study provides validation for PartMC-MOSAIC due to good agreement to field observations. The structure of this manuscript is as follows. Section 2 states the governing equations that form the basis of the model, and Sect. 3 describes the numerical methods. Section 4 shows the ship plume modeling results, and Sect. 5 summarizes our major findings.

2 Coupled equations governing gas-particle interactions

20

Our modeling framework considers a Lagrangian parcel, which simulates the evolution of aerosol particles and trace gases that are emitted by the ship in a volume of air moving along a specified trajectory at the center of the plume. After leaving the exhaust stack the air parcel is not further influenced by emissions. In addition to coagulation
25 and aerosol and gas chemistry within the plume, the model treats mixing of the parcel with background air. Within the air parcel we do not track the physical location of

aerosol particles, and we assume homogeneous meteorological conditions and gas concentrations.

Assuming that an aerosol particle contains mass $\mu_a > 0$ (kg) of species a , for $a = 1, \dots, A$, the particle composition is described by the A -dimensional vector $\boldsymbol{\mu} \in \mathbb{R}^A$. The cumulative aerosol number distribution at time t and constituent masses $\boldsymbol{\mu} \in \mathbb{R}^A$ is $N(\boldsymbol{\mu}, t)$ (m^{-3}), which is defined to be the number concentration of aerosol particles that contain less than μ_a mass of species a , for all $a = 1, \dots, A$. The aerosol number distribution at time t and constituent masses $\boldsymbol{\mu} \in \mathbb{R}^A$ is $n(\boldsymbol{\mu}, t)$ ($\text{m}^{-3} \text{kg}^{-A}$), which is defined by

$$n(\boldsymbol{\mu}, t) = \frac{\partial^A N(\boldsymbol{\mu}, t)}{\partial \mu_1 \partial \mu_2 \dots \partial \mu_A} \quad (1)$$

We denote the concentration of trace gas phase species i at time t by $g_i(t)$ (mol m^{-3}), for $i = 1, \dots, G$, so the trace gas phase species concentrations are described by the G -dimensional vector $\mathbf{g}(t) \in \mathbb{R}^G$. We assume that the aerosol and gas species are numbered so that the first C species of each undergo gas-to-particle conversion, and that they are in the same order so that gas species i converts to aerosol species i , for $i = 1, \dots, C$. Besides, we further assume that aerosol species $C + 1$ is water.

The complete set of differential equations governing the time evolution of the multidimensional aerosol size distribution with gas phase coupling in PartMC-MOSAIC is

Particle-resolved modeling of a ship plume

J. Tian et al.

Title Page

Abstract

Introduction

Conclusions

References

Tables

Figures

◀

▶

◀

▶

Back

Close

Full Screen / Esc

Printer-friendly Version

Interactive Discussion



written in Eqs. (2) and (3),

$$\begin{aligned}
 \frac{\partial n(\boldsymbol{\mu}, t)}{\partial t} = & \underbrace{\frac{1}{2} \int_0^{\mu_1} \int_0^{\mu_2} \dots \int_0^{\mu_A} K(\boldsymbol{\mu}', \boldsymbol{\mu} - \boldsymbol{\mu}') n(\boldsymbol{\mu}', t) n(\boldsymbol{\mu} - \boldsymbol{\mu}', t) d\mu'_1 d\mu'_2 \dots d\mu'_A}_{\text{coagulation gain}} \\
 & - \underbrace{\int_0^{\infty} \int_0^{\infty} \dots \int_0^{\infty} K(\boldsymbol{\mu}, \boldsymbol{\mu}') n(\boldsymbol{\mu}, t) n(\boldsymbol{\mu}', t) d\mu'_1 d\mu'_2 \dots d\mu'_A}_{\text{coagulation loss}} \\
 & + \underbrace{\lambda_{\text{dil}}(t)(n_{\text{back}}(\boldsymbol{\mu}, t) - n(\boldsymbol{\mu}, t))}_{\text{dilution}} - \underbrace{\sum_{i=1}^C \frac{\partial}{\partial \mu_i} (c_i I_i(\boldsymbol{\mu}, \mathbf{g}, t) n(\boldsymbol{\mu}, t))}_{\text{gas-particle transfer}} \\
 & - \underbrace{\frac{\partial}{\partial \mu_{C+1}} (c_w I_w(\boldsymbol{\mu}, \mathbf{g}, t) n(\boldsymbol{\mu}, t))}_{\text{water transfer}} + \underbrace{\frac{1}{\rho_{\text{dry}}(t)} \frac{d\rho_{\text{dry}}(t)}{dt} n(\boldsymbol{\mu}, t)}_{\text{air density change}} \quad (2)
 \end{aligned}$$

$$\begin{aligned}
 \frac{dg_i(t)}{dt} = & \underbrace{\lambda_{\text{dil}}(t)(g_{\text{back},i}(t) - g_i(t))}_{\text{dilution}} + \underbrace{R_i(\mathbf{g})}_{\text{chemical reactions}} + \underbrace{\frac{1}{\rho_{\text{dry}}(t)} \frac{d\rho_{\text{dry}}(t)}{dt} g_i(t)}_{\text{air density change}} \\
 & - \underbrace{\int_0^{\infty} \int_0^{\infty} \dots \int_0^{\infty} I_i(\boldsymbol{\mu}, \mathbf{g}, t) n(\boldsymbol{\mu}, t) d\mu_1 d\mu_2 \dots d\mu_A}_{\text{gas-particle transfer}} \quad (3)
 \end{aligned}$$

In Eq. (2), $K(\boldsymbol{\mu}, \boldsymbol{\mu}')$ ($\text{m}^3 \text{s}^{-1}$) is the coagulation coefficient between particles with constituent masses $\boldsymbol{\mu}$ and $\boldsymbol{\mu}'$, $\lambda_{\text{dil}}(t)$ (s^{-1}) is the dilution rate, $n_{\text{back}}(\boldsymbol{\mu}, t)$ ($\text{m}^{-3} \text{kg}^{-A}$) is the

Particle-resolved modeling of a ship plume

J. Tian et al.

Title Page

Abstract

Introduction

Conclusions

References

Tables

Figures

◀

▶

◀

▶

Back

Close

Full Screen / Esc

Printer-friendly Version

Interactive Discussion



Particle-resolved modeling of a ship plume

J. Tian et al.

Title Page

Abstract

Introduction

Conclusions

References

Tables

Figures

◀

▶

◀

▶

Back

Close

Full Screen / Esc

Printer-friendly Version

Interactive Discussion



background number distribution, c_i (kg mol^{-1}) is the conversion factor from moles of gas species i to mass of aerosol species i (with c_w the factor for water), $I_i(\boldsymbol{\mu}, \mathbf{g}, t)$ (mols^{-1}) is the condensation flux of gas species i (with $I_w(\boldsymbol{\mu}, \mathbf{g}, t)$ the flux for water). In Eq. (3), $g_{\text{back},i}(t)$ (mol m^{-3}) is the background concentration of gas species i , $R_i(\mathbf{g})$ ($\text{mol m}^{-3} \text{s}^{-1}$) is the concentration growth rate of gas species i due to chemical reactions in the gas phase, and $\rho_{\text{dry}}(t)$ (kg m^{-3}) is the dry air density.

To model the dilution process we followed von Glasow et al. (2003) who proposed a Gaussian plume dispersion model for the evolution of the plume in the horizontal and vertical directions. The time-dependent plume width $w_{\text{pl}}(t)$ and height $h_{\text{pl}}(t)$ are described by two power laws as:

$$w_{\text{pl}}(t) = w_0 \left(\frac{t + t_0}{t_0} \right)^\alpha, \quad (4)$$

$$h_{\text{pl}}(t) = h_0 \left(\frac{t + t_0}{t_0} \right)^\beta, \quad (5)$$

where w_0 and h_0 are the dimensions of the plume at the start of the simulation. Note that compared to the formulation in von Glasow et al. (2003) we introduced t_0 in the numerator to avoid a singularity for $t = 0$ in the expression for the dilution rate below. The coefficients α and β are the plume expansion parameters in the horizontal and vertical, respectively. Assuming the plume cross section is semi-elliptic and is given as $A_{\text{pl}} = (\pi/8)w_{\text{pl}}h_{\text{pl}}$, the dilution rate $\lambda_{\text{dil}}(t)$ is:

$$\lambda_{\text{dil}}(t) = \frac{1}{A_{\text{pl}}} \frac{dA_{\text{pl}}}{dt} = \frac{\alpha + \beta}{t + t_0} \quad (6)$$

Previous ship plume studies have estimated the plume width and height at a plume age of 1 s to be approximately 10 m and 5.5 m, respectively (von Glasow et al., 2003; Durkee et al., 2000a; Ferek et al., 1998), and we used these values for t_0 , w_0 and h_0 ,

respectively. The parameters $\alpha = 0.75$ and $\beta = 0.6$ are the “best guesses” estimated from the expansion of ship tracks reported in the literature (von Glasow et al., 2003; Durkee et al., 2000a) and confirmed by observations reported in Petzold et al. (2008).

We further assume the top of the marine boundary layer to be impenetrable by the plume and define z_{MBL} as the height of the marine boundary layer. The total dilution rate used in our ship plume simulation is then written as

$$\lambda_{\text{dil}}(t) = \begin{cases} \frac{\alpha+\beta}{t+t_0} & h_{\text{pl}}(t) < z_{\text{MBL}} \\ \frac{\alpha}{t+t_0} & h_{\text{pl}}(t) = z_{\text{MBL}} \end{cases} \quad (7)$$

3 Numerical implementation

The detailed description of the numerical methods used in PartMC-MOSAIC is given in Riemer et al. (2009). Here we briefly introduce the salient features of the model. PartMC (Particle-resolved Monte Carlo) is a 0-D or box model, which explicitly resolves the composition of many individual particles within a well-mixed computational volume representing a much larger air parcel. During the evolution of the air parcel moving along a specific trajectory, the mass of each constituent species within each particle is tracked. Emission, dilution and Brownian coagulation are simulated with a stochastic Monte Carlo approach. The relative positions of particles within the computational volume are not tracked.

PartMC is coupled with the state-of-the-art aerosol chemistry model MOSAIC (Model for Simulating Aerosol Interactions and Chemistry) (Zaveri et al., 2008) which includes the gas phase photochemical mechanism CBM-Z (Zaveri and Peters, 1999), the Multicomponent Taylor Expansion Method (MTEM) for estimating activity coefficients of electrolytes and ions in aqueous solutions (Zaveri et al., 2005b), the Multicomponent Equilibrium Solver for Aerosols (MESA) for intraparticle solid-liquid partitioning (Zaveri et al., 2005a) and the Adaptive Step Time-split Euler Method (ASTEM) for dynamic gas-particle partitioning over size- and composition-resolved aerosol (Zaveri et al., 2008),

Particle-resolved modeling of a ship plume

J. Tian et al.

Title Page

Abstract

Introduction

Conclusions

References

Tables

Figures

◀

▶

◀

▶

Back

Close

Full Screen / Esc

Printer-friendly Version

Interactive Discussion



**Particle-resolved
modeling of a ship
plume**

J. Tian et al.

Title Page

Abstract

Introduction

Conclusions

References

Tables

Figures

◀

▶

◀

▶

Back

Close

Full Screen / Esc

Printer-friendly Version

Interactive Discussion



as well as a treatment for SOA (secondary organic aerosol) based on the SORGAM scheme (Schell et al., 2001). The CBM-Z gas phase mechanism treats a total of 77 gas species. MOSAIC treats key aerosol species including sulfate (SO_4), nitrate (NO_3), ammonium (NH_4), chloride (Cl), carbonate (CO_3), methanesulfonic acid (MSA), sodium (Na), calcium (Ca), other inorganic mass (OIN), BC, POC, and SOA. OIN represents species such as SiO_2 , metal oxides, and other unmeasured or unknown inorganic species present in aerosols. SOA includes reaction products of aromatic precursors, higher alkenes, α -pinene and limonene.

A challenge of particle-resolved models is the large computational burden when simulating the evolution of particles under ambient conditions. Particle size distributions usually cover a very broad size range from a few nanometers to tens of micrometers, and typically the number concentrations of the small particles compared to the large particles differ by several orders of magnitude. For example, for the simulations presented in this paper, the initial number concentration of the coarse mode was around 10^{10} m^{-3} and approximately 10^{15} m^{-3} in the volatile nucleation mode (see Table 3). Both sub-populations are important as the small particles dominate particle number concentration whereas the large particles dominate particle mass concentrations. Moreover, the most likely coagulation events involve interactions of small and large particles. It is challenging to represent such a particle distribution with a particle-resolved model, so that the large, rare particles are sufficiently resolved, while the overall number of computational particles is still manageable. Here we used the method by DeVille et al. (2011) and DeVille et al. (2013) to reduce the computational cost and improve the model efficiency. This method is based on the notion that a single computational particle can correspond to some number of real particles, in other words, each computational particle is “weighted” by an appropriate factor. We computationally over-represent the rare but important particles and underrepresent the common particles. With this approach it is possible to span the large range of sizes and abundances of the particle population as will be demonstrated in Sect. 4.

of both particle composition and diameter. The two-dimensional cumulative number distribution $N_{a,\text{dry}}(D, w)$ is the number of particles per volume that have a diameter less than D and a dry mass fraction less than w for certain species a . Here a could be BC, POC, sulfate, nitrate, etc. The two-dimensional number distribution $n_{a,\text{dry}}(D, w)$ is then defined by

$$n_{a,\text{dry}}(D, w) = \frac{\partial^2 N_{a,\text{dry}}(D, w)}{\partial \log_{10} D \partial w} \quad (11)$$

Similarly, we can define a two-dimensional number distribution $n_{\text{coag}}(D, k)$ based on the number of coagulation events k that a given particle has experienced during the simulation time. Let $N_{\text{coag}}(D, k)$ be the cumulative number distribution describing the number of particles per volume with diameter less than D and that have experienced less than k coagulation events, $n_{\text{coag}}(D, k)$ can be written as

$$n_{\text{coag}}(D, k) = \frac{\partial N_{\text{coag}}(D, k)}{\partial \log_{10} D \partial k} \quad (12)$$

To investigate changes in the CCN properties of the aerosols, we use the hygroscopicity parameter κ to define a two-dimensional cumulative number distribution $N_{\kappa}(D, \kappa)$ in terms of diameter and hygroscopicity parameter. Then the two-dimensional number distribution is written as

$$n_{\kappa}(D, \kappa) = \frac{\partial^2 N_{\kappa}(D, \kappa)}{\partial \log_{10} D \partial \log_{10} \kappa} \quad (13)$$

3.2 CCN activity module

The unique feature of PartMC-MOSAIC to provide particle-resolved mixing state information enables us to calculate the critical supersaturation $S_{c,i}$ that an individual particle

Particle-resolved modeling of a ship plume

J. Tian et al.

Title Page

Abstract

Introduction

Conclusions

References

Tables

Figures

◀

▶

◀

▶

Back

Close

Full Screen / Esc

Printer-friendly Version

Interactive Discussion



requires to activate. The procedure is as follows. The per-particle water activity $a_{w,i}$ is given by:

$$\frac{1}{a_{w,i}} = 1 + \kappa_i \frac{V_{\text{dry},i}}{V_{w,i}} \quad (14)$$

where κ_i is a single, dimensionless hygroscopicity parameter to relate particle dry diameter to CCN activity (Ghan et al., 2001; Petters and Kreidenweis, 2007), $V_{\text{dry},i}$ is the dry particle volume and $V_{w,i}$ is the volume of water in the particle. For an aerosol particle i containing several non-water species, the κ_i value for the particle is the volume-weighted mean of the individual κ value of each constituent species (Petters and Kreidenweis, 2007). Table 1 lists κ values for individual aerosol components used in this study. The equilibrium saturation ratio $S(D_i)$ over an aqueous particle i is given by the Köhler equation:

$$S(D_i) = a_{w,i} \exp\left(\frac{4\sigma_w M_w}{RT \rho_w D_i}\right) \quad (15)$$

where σ_w is the surface tension of the solution–air interface, M_w is the molecular weight of water, R is the universal gas constant, T is the temperature, and D_i is the particle wet diameter. Combining Eqs. (14) and (15) and using wet and dry diameters D_i and $D_{\text{dry},i}$ to represent their respective volumes, we obtain the κ -Köhler equation based on Petters and Kreidenweis (2007):

$$S(D_i) = \frac{D_i^3 - D_{\text{dry},i}^3}{D_i^3 - D_{\text{dry},i}^3(1 - \kappa_i)} \exp\left(\frac{4\sigma_w M_w}{RT \rho_w D_i}\right) \quad (16)$$

To calculate the critical supersaturation, we set $\partial S(D_i)/\partial D_i$ to zero and numerically solve for the critical wet diameter D_i , then use Eq. (16) to obtain the critical supersaturation $S_{c,i}$ for each particle.

Particle-resolved modeling of a ship plume

J. Tian et al.

Title Page

Abstract

Introduction

Conclusions

References

Tables

Figures

◀

▶

◀

▶

Back

Close

Full Screen / Esc

Printer-friendly Version

Interactive Discussion



3.3 Setup of case study

Measurements of the particle and gas phase of the raw engine exhaust served as initial input parameters for our model runs. To evaluate our model, the output was compared to measurements performed in a single ship plume and in a ship corridor study. The two campaigns are briefly described in the following section. Details can be found in Petzold et al. (2008, 2010) and Pfaffenberger et al. (2013).

The initial concentrations of gases and particles as well as particle size distribution and composition were obtained from the HERCULES study in 2006 during which a serial four stroke marine diesel engine was used on a test rig (Petzold et al., 2008, 2010). The heavy fuel oil was composed of 86.9 weight-% carbon, 10.4 weight-% hydrogen, 2.21 weight-% sulphur, and some minor constituents. We used the exhaust data under 75 % engine load condition for our model inputs. The aerosol size distribution present in the raw engine exhaust served as input for the model initialization.

Within the QUANTIFY SHIPS field study in June 2007, airborne measurements of a single ship plume as well as aged aerosol in highly frequented sea lanes were performed. As in-plume total particle number concentrations we considered the maximum measured concentration during one plume crossing ($D > 4$ nm). Size distributions of both the polluted and the clean marine boundary layer were determined using a combination of instruments capable of measuring in different size ranges. Last but not least, the following meteorological parameters in the well-mixed marine boundary layer were measured and used for the model runs: a relative humidity of $RH = 90$ %, a temperature $T = 289$ K and a boundary layer mixing height $z_{MBL} = 300$ m.

Table 2 shows the initial and background conditions of the gaseous species obtained from the airborne measurements during the HERCULES and QUANTIFY study, respectively. From the HERCULES measurements only the total amount of non-methane hydrocarbons (NMHC) was known. The attribution to the various model species of the CBM-Z gas phase mechanism were based on results from Eyring et al. (2005).

Particle-resolved modeling of a ship plume

J. Tian et al.

Title Page

Abstract

Introduction

Conclusions

References

Tables

Figures

◀

▶

◀

▶

Back

Close

Full Screen / Esc

Printer-friendly Version

Interactive Discussion



**Particle-resolved
modeling of a ship
plume**

J. Tian et al.

Title Page

Abstract

Introduction

Conclusions

References

Tables

Figures



Back

Close

Full Screen / Esc

Printer-friendly Version

Interactive Discussion



Table 3 shows the total number concentration, count median diameter and geometric standard deviation, the parameters determining the initial, background and ship corridor size distributions. The initial aerosol size distribution from the test rig study was composed of three distinct modes with one volatile nucleation mode and two larger combustion modes. The volatile mode consisted of 100 % sulfate, while BC, POC and ash were present in the two combustion modes. The background aerosol distribution was tri-modal with Aitken, accumulation and coarse modes. We assigned the fractions of sulfate, ammonium, nitrate, POC, BC and sea salt to these three modes based on O'Dowd and De Leeuw (2007).

We initialized our model with 10^5 computational particles and followed the air parcel as it evolved for 14 h to predict the aged plume and to compare to measurements from the ship corridor. For the base case, the simulation started at 2 p.m. LT, similar to the measurement time of the single plume study on 14 June in 2007. During the plume evolution we considered the following processes: dilution with the background air, coagulation of the particles, chemical transformations in the aerosol and gas phase, and phase transitions. Since coagulation of two particles may physically or thermodynamically change the resulting particles' composition and phase state, and subsequently alter the CCN activation properties, we carried out another simulation with coagulation switched off. Furthermore, due to the stochastic nature of PartMC-MOSAIC, for each simulation we conducted an ensemble of 10 runs and averaged the results of these runs to obtain more robust statistics. To quantify the variability within this ensemble, we show the 95 % confidence interval for the size distributions in Figs. 3 and 4 below.

We also simulated a sensitivity case by setting the model starting time to 6 a.m. LT instead of 2 p.m., to investigate conditions with a longer exposure to sunlight and hence more opportunity for secondary aerosol mass formation. Analogous to the base case we performed the sensitivity case including coagulation and neglecting coagulation.

4 Results and discussion

In this section we present the results of our base case simulation of the ship plume (start at 2 p.m. LT), and contrast it with the sensitivity case (start at 6 a.m. LT). To provide context, we begin by discussing the simulated evolution of selected trace gas species and bulk aerosol species. We then show the comparison of measured and modeled total number concentrations from a single plume event, as well as the comparison of measured and modeled size distributions from the shipping corridor. Finally, we quantify the role of coagulation for the evolution of aerosol mixing state and its impacts on CCN properties.

4.1 Evolution of gas and bulk aerosol species

Figure 1 shows the evolution of key trace gas mixing ratios and bulk aerosol species concentrations in the ship plume as it evolves for 14 h. For our base case (start at 2 p.m. LT), dilution reduced the concentrations of the primary emitted species by several orders of magnitude within the first 15–20 min of simulation time. Ozone was diluted in from the background air. For the base case the transition from day to night occurred at about 6 h after the simulation started. The NO_2 mixing ratio was further decreased after 6 h due to nighttime chemistry to form reservoir species such as dinitrogen pentoxide (N_2O_5). The OH mixing ratio reached about 0.03 ppt after 2 h of simulation and decreased later in the afternoon. The HNO_3 mixing ratio reached quickly its background value within the first 10 min, then showed a slight increase during daytime as a result of photochemical processes, and a subsequent decrease due to reaction with sea salt to form sodium nitrate.

Similar to the primary gaseous species, sulfate and BC started out with high initial mass concentrations and were depleted very quickly due to dilution. There was no net formation of sulfate mass during plume aging since dilution dominated the evolution of total sulfate mass concentration. Note that our predicted sulfate concentration may be underestimated since we did not include vanadium-catalyzed sulfate production

Particle-resolved modeling of a ship plume

J. Tian et al.

Title Page

Abstract

Introduction

Conclusions

References

Tables

Figures

◀

▶

◀

▶

Back

Close

Full Screen / Esc

Printer-friendly Version

Interactive Discussion



reactions in our model, as proposed by Ault et al. (2010). The SOA concentrations increased only by about $0.01 \mu\text{g m}^{-3}$. The lack of production of secondary aerosol mass was a result of the low OH concentrations in the plume, so that oxidation reactions were largely limited. Our finding is consistent with the results reported in Hobbs et al. (2000), where they did not observe any appreciable increase of the aerosol mass concentration in the ship plume with similar initial conditions and sun light exposure time.

The sensitivity case (start at 6 a.m. LT) shows an OH mixing ratio 10 times higher than in the original run, and the corresponding SOA mass concentration was enhanced by a factor of 10. An increase of sulfate mass concentration was observed after 4 h of simulation, leading to a net production of sulfate mass concentration in the plume of about $2 \mu\text{g m}^{-3}$. This shows as expected that the production of secondary aerosol species is largely determined by the exposure time to sunlight during daytime.

4.2 Evolution of total number concentration in a single plume

Figure 2 compares our predicted total particle number concentrations to those measured in a ship plume during the single plume study on 14 June 2007. The measurements were taken within the first hour after the ship emissions entered the atmosphere, representing a relatively fresh plume. The horizontal error bars on the measured values show the estimated errors in determining plume ages. The estimated relative errors in number concentration are less than 8%, and are not visible in this graph due to the logarithmic scaling of the ordinate. As described in Sect. 3.3 we initialized the model simulations with data from the HERCULES study, indicated here with the red dot. The modeled time series of number concentration shows a sharp decrease at the beginning due to dilution and coagulation, and then the model results approach the measurements well when coagulation is included (red line). When coagulation was not simulated, the total particle number concentration was overestimated by a factor of ten (blue line). Note that since the plume encounter times during the measurements were very short, neither size distribution nor chemical composition data could be obtained from the single plume study.

Particle-resolved modeling of a ship plume

J. Tian et al.

Title Page

Abstract

Introduction

Conclusions

References

Tables

Figures

◀

▶

◀

▶

Back

Close

Full Screen / Esc

Printer-friendly Version

Interactive Discussion



4.3 Evolution of particle size distributions in the shipping corridor

The aerosol population measured in the shipping corridor can be thought of as the superposition of many ship plumes of different, however unknown, ages. This makes it difficult to compare the size distribution measurements quantitatively to the model results, which simulate only one specific plume. Here we attempt to use the observations for a qualitative comparison to see if the PartMC-MOSAIC results are consistent with the observations.

Figure 3 displays the in-plume aerosol number distributions for the base case. The red, green and blue curves represent the measured aerosol distributions for initial, background and ship corridor conditions, while the five black curves are the predicted distributions at plume ages of 100 s, 1200 s, 1 h, 5 h and 14 h, respectively. All the model results are the averages of an ensemble of 10 runs. The error bars represent the 95 % confidence intervals, only shown for size distribution at 100 s as an example. These are vanishingly small for small particle sizes and are somewhat larger for the size range above 500 nm. This is a result of the fact that less computational particles are used to represent the larger sizes (even with using the weighted particle algorithm as described in Sect. 3).

To illustrate the effect of coagulation on particle size distributions, we show both the simulation results without coagulation (Fig. 3a) and with coagulation (Fig. 3b). Figure 3a shows that particle number concentration was significantly reduced due to dilution within the first 100 s, but simultaneously large particles from background were diluted into the plume so that an accumulation and a coarse mode in the size distributions were formed.

However it is obvious that the shape of the size distribution observed in the shipping corridor could not be reproduced when coagulation was neglected. The predicted number concentration of small particles was overestimated compared to the ship corridor measurement. For example, at 14 h, PartMC-MOSAIC overpredicted the number con-

Particle-resolved modeling of a ship plume

J. Tian et al.

Title Page

Abstract

Introduction

Conclusions

References

Tables

Figures



Back

Close

Full Screen / Esc

Printer-friendly Version

Interactive Discussion



centration of particles with sizes 30 nm by at least one order of magnitude compared to the observed value.

When coagulation was included (Fig. 3b), the depletion of the small particles in the volatile mode was captured and the modeled and observed size distributions agreed qualitatively better. Due to the short daylight exposure time the particle growth owing to condensation of secondary aerosol was small for this simulation, as already pointed out in the discussion of Fig. 1. Therefore, in this case, coagulation and dilution were the driving processes that shaped the size distributions.

To investigate the impact of daylight exposure time further, Fig. 4 shows the in-plume particle size distributions for the simulation of the sensitivity case, with a simulation start of 6 a.m. The size distributions of plume ages smaller than 1 h were similar to those for the base case. However in the more aged plume (at 5 h and 14 h), condensation of secondary aerosol mass set in, which shifted the particles to larger sizes. As in Fig. 3, we see that including coagulation led to particle size distributions that are qualitatively in better agreement with the observations.

Overall, Figs. 3 and 4 demonstrate that dilution and coagulation were the two major processes dominating the evolution of particles in ship plumes. While dilution significantly reduced the overall in-plume number concentrations, coagulation reduced the number concentrations of the small volatile particles. Moreover, the growth of particles was sensitive to the start of the simulation time. An earlier starting time with a longer, and more intense sun exposure enhanced the production of secondary aerosol mass. Generally, our model results are qualitatively consistent with the observations in the shipping corridor.

4.4 Impact of coagulation on particle mixing state

To elucidate how the mixing state evolved over the course of the simulation of the base case, we show the two-dimensional number distribution as a function of dry diameter and dry mass fraction of BC and sulfate in Fig. 5 at plume ages of 100 s, 1 h and 5 h. The simulation results including coagulation and neglecting coagulation are placed next

Particle-resolved modeling of a ship plume

J. Tian et al.

Title Page

Abstract

Introduction

Conclusions

References

Tables

Figures



Back

Close

Full Screen / Esc

Printer-friendly Version

Interactive Discussion



to each other for comparison. The definition of the two-dimensional number distribution function is given in Sect. 3.1.

BC initially resided in the two combustion aerosol modes and also to a small extent in the background aerosol mode. Without coagulation (Fig. 5a, e, and i), the three particle source types were at all times distinctly separated shown as horizontal bands in the two-dimensional number distribution plot. However, when coagulation was included (Fig. 5b, f, and j), a continuum of internal mixing states was established very quickly with BC dry mass fraction ranging from 0 to 12 %.

An analogous evolution of the sulfate mixing state was observed. A continuum of internal mixtures from 0 to 100 % of sulfate dry mass fraction formed due to coagulation (Fig. 5d, h, and l), while for the simulation without coagulation the particles from different sources remained externally mixed (Fig. 5c, g, and k). An interesting feature of the sulfate mixing state is that after 1 h, the previously horizontal lines representing the particles from various sources became “tilted” (Fig. 5g, h, k and l). This tilt formed because secondary aerosol mass condensed on the particles, and the resulting change in sulfate dry mass fraction was relatively larger for small particles compared to large particles. For the volatile-mode particles the tilt was the result of ammonia partitioning into the aerosol phase and thereby reducing the sulfate dry mass fraction. In our simulation ammonia originated from the evaporation of ammonium nitrate present in the background particles. For the combustion-mode particles the tilt was due to the condensation of sulfuric acid, thereby increasing the sulfate dry mass fraction. This two-way condensation effect on sulfate mixing state was observed in both simulations with and without coagulation. A similar behavior could also be observed for the BC mixing state (e.g. Fig. 5i and j).

Given that coagulation is such an important process in the ship plume, it is interesting to explore the number of coagulation events experienced by the individual particles as the plume evolves. Figure 6 shows the two-dimensional number distribution $n_{\text{coag}}(D, k)$ at plume ages of 100 s, 1 h, 5 h and 14 h, where k is the number of coagulation events. At early plume age (100 s), the peak around 0.1 μm indicates intense coagulation be-

Particle-resolved modeling of a ship plume

J. Tian et al.

Title Page

Abstract

Introduction

Conclusions

References

Tables

Figures

◀

▶

◀

▶

Back

Close

Full Screen / Esc

Printer-friendly Version

Interactive Discussion



Particle-resolved modeling of a ship plume

J. Tian et al.

Title Page

Abstract

Introduction

Conclusions

References

Tables

Figures

◀

▶

◀

▶

Back

Close

Full Screen / Esc

Printer-friendly Version

Interactive Discussion



tween particles from volatile and combustion-1 modes. As time evolved, another peak at $0.2\ \mu\text{m}$ appeared, representing background accumulation mode particles. It can be deduced from Fig. 6 that particles below $0.1\ \mu\text{m}$ experienced more coagulation events as particle size increased. This reflects the fact that small particles disappear and larger particles survive in the plume during coagulation. The same behavior was also observed for the coarse mode, which was mainly composed of background particles. Given a certain particle size, the number of coagulation events varied, which shows the stochastic nature of the coagulation process. This variation also increased dramatically with size, for example, while the number of coagulation events varied between 0 and 15 for particles with $D = 0.04\ \mu\text{m}$, it ranged between 0 and 100 for particles with $D = 0.1\ \mu\text{m}$ at plume age of 14 h.

4.5 Cloud condensation nuclei activity

We will now address the question to what extent the changes in aerosol mixing state translated into changes in CCN activity. For this purpose it is convenient to display the number distribution $n_\kappa(D, \kappa)$ based on Eq. (13), as shown in Fig. 7 for 0 s, 100 s, 1 h and 5 h (base case simulation, including coagulation). Initially ($t = 0\ \text{s}$), three distinct bands represented the volatile and the two combustion modes. The position of each band was determined by the initial composition of each mode determining the overall hygroscopicity. The volatile-mode particles, which contained 100 % sulfate, had the largest hygroscopicity, while hydrophobic combustion-1-mode particles, consisting of POC and BC, were most difficult to activate initially.

At $t = 100\ \text{s}$, the space between the three bands had begun to fill out due to coagulation and the associated change of mixing state. As a result, for a subset of the combustion mode particles the hygroscopicity parameter increased. After 1 h and 5 h, the average κ values of the aerosol population increased further, indicating that a larger fraction of the particles had the potential to become a CCN for a certain supersaturation threshold. Note that particles larger than $0.2\ \mu\text{m}$ represented mainly the background particles, as shown in Fig. 3.

**Particle-resolved
modeling of a ship
plume**

J. Tian et al.

Title Page

Abstract

Introduction

Conclusions

References

Tables

Figures

◀

▶

◀

▶

Back

Close

Full Screen / Esc

Printer-friendly Version

Interactive Discussion



Figure 8 shows the evolution of CCN concentration for three different supersaturation thresholds ($S = 0.1\%$, $S = 0.3\%$, $S = 0.6\%$), denoted by CCN(0.1), CCN(0.3), CCN(0.6). We also show the corresponding simulations including coagulation and neglecting coagulation to quantify the impact of this process on CCN concentrations. As seen in Fig. 5 and Fig. 7, rather than increasing the particle size, coagulation significantly altered the mixing state of particles and increased the particle hygroscopicity of initially hydrophobic particles. Coagulation therefore may enhance the CCN number concentrations, while decreasing the total particle number concentration. However, the magnitude of the CCN concentration enhancement depended on the threshold of environmental supersaturation as well as on the amount of secondary aerosol mass that condensed on the particles.

For the base case (Fig. 8a) at 14 h, the CCN(0.1) concentration was 82 cm^{-3} , CCN(0.3) was 484 cm^{-3} , and CCN(0.6) was 1240 cm^{-3} when coagulation was included. The CCN(0.3) concentration decreased by about 200 cm^{-3} (44 % reduction), and the CCN(0.6) concentration decreased by 300 cm^{-3} (22 % reduction) when coagulation was neglected. Interestingly, coagulation did not affect the CCN(0.1) concentration. This means that coagulation of combustion particles with sulfate particles was not sufficient to increase the hygroscopicity of the combustion particles to the extent that they could activate at such a low supersaturation level.

This picture changed for the sensitivity case (Fig. 8b), which was characterized by increased formation of secondary aerosol mass compared to the base case. For this case CCN concentrations increased during the afternoon for all S , and for both the simulations including and neglecting coagulation. An exception is the time series for CCN(0.6) for the simulation including coagulation. Here we do not observe an increase in the afternoon because the ratio CCN/CN reached almost 1 around noon, i.e. almost all particles activated at that time, and further condensation of secondary aerosol material did not lead to any further increase of CCN. In contrast, when coagulation was neglected, CCN(0.6) reached higher values compared to the run with coagulation, because the aerosol number concentration was higher and because condensational

growth brought these particles to sizes so that activation was possible. Further, for the sensitivity case coagulation did have an impact on CCN(0.1) concentration, which decreased by about 42 % when coagulation was neglected. This means that the condensation of secondary aerosol increased the hygroscopicity of the combustion particles enough, so that some of them could activate at $S = 0.1$ %. Then, the CCN(0.1) concentration could be modulated further by coagulation between combustion and sulfuric acid particles.

It has been reported that the typical supersaturation for marine stratocumulus is around 0.1 % (Hoppel et al., 1996; Martucci and O'Dowd, 2011). Our results of CCN(0.1) concentration suggest that the influence of coagulation on marine cloud formation will significantly depend on the time of the day that ship-emitted particles are exposed to the marine boundary layer.

5 Conclusions

In this paper we presented the application of the stochastic aerosol model PartMC-MOSAIC to investigate the evolution of aerosol mixing state and associated changes of CCN properties in a ship plume. This work provides the first validation study of PartMC, and we showed that the model results agreed well with observed particle number concentrations and size distributions.

From our process analysis we conclude that dilution and coagulation were the two major processes influencing the particle distribution and the resulting CCN activation properties. Dilution reduced the in-plume total particle number concentration by about four orders of magnitude within 15 min from simulation start. Coagulation further reduced the particle number concentration by another order of magnitude and preferentially depleted small volatile particles. To adequately capture the evolution of the size distribution, it was essential to include coagulation.

Moreover, coagulation altered the particle mixing state in the fresh plume, leading to internally mixed aerosols containing BC and sulfate within the first 1–2 min after emis-

Particle-resolved modeling of a ship plume

J. Tian et al.

Title Page

Abstract

Introduction

Conclusions

References

Tables

Figures



Back

Close

Full Screen / Esc

Printer-friendly Version

Interactive Discussion



Particle-resolved modeling of a ship plume

J. Tian et al.

Title Page

Abstract

Introduction

Conclusions

References

Tables

Figures

◀

▶

◀

▶

Back

Close

Full Screen / Esc

Printer-friendly Version

Interactive Discussion



sion. This impacted the CCN properties even for conditions when only small amounts of hygroscopic secondary aerosol mass were formed, as it applied for our base case simulation. However, the impact depended on the supersaturation threshold. Neglecting coagulation reduced the CCN number concentration for the base case by 200 cm^{-3} (or 44 %) and 300 cm^{-3} (or 22 %) for supersaturation thresholds of 0.3 % and 0.6 %, respectively. However, at a supersaturation threshold of 0.1 %, the CCN concentration was not impacted by coagulation. The amount of sulfate added to the combustion particles by coagulation was not sufficient to render them CCN active at $S = 0.1\%$. For conditions with higher formation rates of secondary aerosol mass, coagulation did have an impact on CCN concentration even at low supersaturation levels. This was shown with our sensitivity case where CCN concentrations were underestimated by 42 % when coagulation was neglected.

Acknowledgements. J. Tian and N. Riemer acknowledge funding from the National Science Foundation (NSF) under Grant CMG-0934491. This publication was made possible by US EPA grant 83504201. Its contents are solely the responsibility of the grantee and do not necessarily represent the official views of the US EPA. Further, US EPA does not endorse the purchase of any commercial products or services mentioned in the publication. Part of this work was supported by the EU FP6 Integrated Project QUANTIFY (Quantifying the Climate Impact of Global and European Transport Systems; <http://www.pa.op.dlr.de/quantify/>).

References

- Agrawal, H., Eden, R., Zhang, X., Fine, P. M., Katzenstein, A., Miller, J. W., Ospital, J., Teffera, S., and Cocker III, D. R.: Primary particulate matter from ocean-going engines in the southern California air basin, *Environ. Sci. Technol.*, 43, 5398–5402, doi:10.1021/es8035016, 2009. 16735
- Ault, A. P., Moore, M. J., Furutani, H., and Prather, K. A.: Impact of emissions from the Los Angeles port region on San Diego air quality during regional transport events, *Environ. Sci. Technol.*, 43, 3500–3506, doi:10.1021/es8018918, 2009. 16734

**Particle-resolved
modeling of a ship
plume**

J. Tian et al.

Title Page

Abstract

Introduction

Conclusions

References

Tables

Figures

◀

▶

◀

▶

Back

Close

Full Screen / Esc

Printer-friendly Version

Interactive Discussion



- Ault, A. P., Gaston, C. J., Wang, Y., Dominguez, G., Thiemens, M. H., and Prather, K. A.: Characterization of the single particle mixing state of individual ship plume events measured at the Port of Los Angeles, *Environ. Sci. Technol.*, 44, 1954–1961, doi:10.1021/es902985h, 2010. 16735, 16749
- 5 Capaldo, K., Corbett, J., Kasibhatla, P., Fischbeck, P., and Pandis, S.: Effects of ship emissions on sulphur cycling and radiative climate forcing over the ocean, *Nature*, 400, 743–746, 1999. 16734, 16735
- Coakley, J., Bernstein, R., and Durkee, P.: Effect of ship-stack effluents on cloud reflectivity, *Science*, 237, 1020–1022, doi:10.1126/science.237.4818.1020, 1987. 16735
- 10 Coggon, M. M., Sorooshian, A., Wang, Z., Metcalf, A. R., Frossard, A. A., Lin, J. J., Craven, J. S., Nenes, A., Jonsson, H. H., Russell, L. M., Flagan, R. C., and Seinfeld, J. H.: Ship impacts on the marine atmosphere: insights into the contribution of shipping emissions to the properties of marine aerosol and clouds, *Atmos. Chem. Phys.*, 12, 8439–8458, doi:10.5194/acp-12-8439-2012, 2012. 16735
- 15 Conover, J.: Anomalous cloud lines, *J. Atmos. Sci.*, 23, 778–785, doi:10.1175/1520-0469(1966)023<0778:ACL>2.0.CO;2, 1966. 16735
- Cooper, D.: Exhaust emissions from ships at berth, *Atmos. Environ.*, 37, 3817–3830, doi:10.1016/S1352-2310(03)00446-1, 2003. 16735
- 20 Corbett, J. J., Winebrake, J. J., Green, E. H., Kasibhatla, P., Eyring, V., and Lauer, A.: Mortality from ship emissions: a global assessment, *Environ. Sci. Technol.*, 41, 8512–8518, doi:10.1021/es071686z, 2007. 16734
- DeVile, R., Riemer, N., and West, M.: Weighted Flow Algorithms (WFA) for stochastic particle coagulation, *J. Computational Phys.*, 230, 8427–8451, doi:10.1016/j.jcp.2011.07.027, 2011. 16742
- 25 DeVile, R., Riemer, N., and West, M.: Convergence of a generalized weighted flow algorithm (WFA) for stochastic particle coagulation, in preparation, 2013. 16742
- Dominguez, G., Jackson, T., Brothers, L., Barnett, B., Nguyen, B., and Thiemens, M. H.: Discovery and measurement of an isotopically distinct source of sulfate in Earth's atmosphere, *Proc. Natl. Acad. Sci. USA*, 105, 12769–12773, doi:10.1073/pnas.0805255105, 2008. 16735
- 30 Durkee, P., Chartier, R., Brown, A., Trehubenko, E., Rogerson, S., Skupniewicz, C., Nielsen, K., Platnick, S., and King, M.: Composite ship track characteristics, *J. Atmos. Sci.*, 57, 2542–2553, doi:10.1175/1520-0469(2000)057<2542:CSTC>2.0.CO;2, 2000a. 16735, 16740, 16741

Particle-resolved modeling of a ship plume

J. Tian et al.

Title Page

Abstract

Introduction

Conclusions

References

Tables

Figures

◀

▶

◀

▶

Back

Close

Full Screen / Esc

Printer-friendly Version

Interactive Discussion



- Durkee, P., Noone, K., and Bluth, R.: The Monterey Area Ship Track experiment, *J. Atmos. Sci.*, 57, 2523–2541, doi:10.1175/1520-0469(2000)057<2523:TMASTE>2.0.CO;2, 2000b. 16735
- Endresen, O., Sorgard, E., Sundet, J., Dalsoren, S., Isaksen, I., Berglen, T., and Gravir, G.: Emission from international sea transportation and environmental impact, *J. Geophys. Res.-Atmos.*, 108, 4560, doi:10.1029/2002JD002898, 2003. 16734
- Erlick, C., Russell, L., and Ramaswamy, V.: A microphysics-based investigation of the radiative effects of aerosol-cloud interactions for two MAST Experiment case studies, *J. Geophys. Res.-Atmos.*, 106, 1249–1269, doi:10.1029/2000JD900567, 2001. 16736
- Eyring, V., Köhler, H., van Aardenne, J., and Lauer, A.: Emissions from international shipping: 1. The last 50 years, *J. Geophys. Res.-Atmos.*, 110, D17305, doi:10.1029/2004JD005619, 2005. 16746, 16764
- Eyring, V., Stevenson, D. S., Lauer, A., Dentener, F. J., Butler, T., Collins, W. J., Ellingsen, K., Gauss, M., Hauglustaine, D. A., Isaksen, I. S. A., Lawrence, M. G., Richter, A., Rodriguez, J. M., Sanderson, M., Strahan, S. E., Sudo, K., Szopa, S., van Noije, T. P. C., and Wild, O.: Multi-model simulations of the impact of international shipping on Atmospheric Chemistry and Climate in 2000 and 2030, *Atmos. Chem. Phys.*, 7, 757–780, doi:10.5194/acp-7-757-2007, 2007. 16734
- Eyring, V., Isaksen, I. S. A., Berntsen, T., Collins, W. J., Corbett, J. J., Endresen, O., Grainger, R. G., Moldanova, J., Schlager, H., and Stevenson, D. S.: Transport impacts on atmosphere and climate: shipping, *Atmos. Environ.*, 44, 4735–4771, doi:10.1016/j.atmosenv.2009.04.059, 2010. 16734
- Ferek, R., Hegg, D., Hobbs, P., Durkee, P., and Nielsen, K.: Measurements of ship-induced tracks in clouds off the Washington coast, *J. Geophys. Res.-Atmos.*, 103, 23199–23206, doi:10.1029/98JD02121, 1998. 16740
- Frick, G. and Hoppel, W.: Airship measurements of ship's exhaust plumes and their effect on marine boundary layer clouds, *J. Atmos. Sci.*, 57, 2625–2648, doi:10.1175/1520-0469(2000)057<2625:AMOSSE>2.0.CO;2, 2000. 16735
- Ghan, S., Laulainen, N., Easter, R., Wagener, R., Nemesure, S., Chapman, E., Zhang, Y., and Leung, R.: Evaluation of aerosol direct radiative forcing in MIRAGE, *J. Geophys. Res.-Atmos.*, 106, 5295–5316, doi:10.1029/2000JD900502, 2001. 16745
- González, Y., Rodríguez, S., Guerra García, J. C., Luis Trujillo, J., and García, R.: Ultrafine particles pollution in urban coastal air due to ship emissions, *Atmos. Environ.*, 45, 4907–4914, doi:10.1016/j.atmosenv.2011.06.002, 2011. 16734

**Particle-resolved
modeling of a ship
plume**

J. Tian et al.

Title Page

Abstract

Introduction

Conclusions

References

Tables

Figures

◀

▶

◀

▶

Back

Close

Full Screen / Esc

Printer-friendly Version

Interactive Discussion



- Hobbs, P. V., Garrett, T. J., Ferek, R. J., Strader, S. R., Hegg, D. A., Frick, G. M., Hoppel, W. A., Gasparovic, R. F., Russell, L. M., Johnson, D. W., O'Dowd, C., Durkee, P. A., Nielsen, K. E., and Innis, G.: Emissions from ships with respect to their effects on cloud, *J. Atmos. Sci.*, 57, 2570–2590, 2000. 16749
- 5 Hoppel, W., Frick, G., and Fitzgerald, J.: Deducing droplet concentration and supersaturation in marine boundary layer clouds from surface aerosol measurements, *J. Geophys. Res.-Atmos.*, 101, 26553–26565, 1996. 16755
- Jacobson, M. Z., Wilkerson, J. T., Naiman, A. D., and Lele, S. K.: The effects of aircraft on climate and pollution, Part I: Numerical methods for treating the subgrid evolution of discrete size- and composition-resolved contrails from all commercial flights worldwide, *J. Comput. Phys.*, 230, 5115–5132, doi:10.1016/j.jcp.2011.03.031, 2011. 16735
- 10 Kasper, A., Aufdenblatten, S., Forss, A., Mohr, M., and Burtscher, H.: Particulate emissions from a low-speed marine diesel engine, *Aerosol Sci. Tech.*, 41, 24–32, doi:10.1080/02786820601055392, 2007. 16735
- 15 Keene, W. C., Stutz, J., Pszenny, A. A. P., Maben, J. R., Fischer, E. V., Smith, A. M., von Glasow, R., Pechtl, S., Sive, B. C., and Varner, R. K.: Inorganic chlorine and bromine in coastal New England air during summer, *J. Geophys. Res.-Atmos.*, 112, D10S12, doi:10.1029/2006JD007689, 2007. 16764
- Lauer, A., Eyring, V., Hendricks, J., Jöckel, P., and Lohmann, U.: Global model simulations of the impact of ocean-going ships on aerosols, clouds, and the radiation budget, *Atmos. Chem. Phys.*, 7, 5061–5079, doi:10.5194/acp-7-5061-2007, 2007. 16735
- 20 Lawrence, M. and Crutzen, P.: Influence of NO_x emissions from ships on tropospheric photochemistry and climate, *Nature*, 402, 167–170, doi:10.1038/46013, 1999. 16734
- Martucci, G. and O'Dowd, C. D.: Ground-based retrieval of continental and marine warm cloud microphysics, *Atmos. Meas. Tech.*, 4, 2749–2765, doi:10.5194/amt-4-2749-2011, 2011. 16755
- 25 Moldanová, J., Fridell, E., Popovicheva, O., Demirdjian, B., Tishkova, V., Faccinnetto, A., and Focsa, C.: Characterisation of particulate matter and gaseous emissions from a large ship diesel engine, *Atmos. Environ.*, 43, 2632–2641, 2009. 16734
- 30 Murphy, S. M., Agrawal, H., Sorooshian, A., Padro, L. T., Gates, H., Hersey, S., Welch, W. A., Jung, H., Miller, J. W., Cocker III, D. R., Nenes, A., Jonsson, H. H., Flagan, R. C., and Seinfeld, J. H.: Comprehensive simultaneous shipboard and airborne characterization of

**Particle-resolved
modeling of a ship
plume**

J. Tian et al.

Title Page

Abstract

Introduction

Conclusions

References

Tables

Figures

◀

▶

◀

▶

Back

Close

Full Screen / Esc

Printer-friendly Version

Interactive Discussion

exhaust from a modern container ship at sea, *Environ. Sci. Technol.*, 43, 4626–4640, doi:10.1021/es802413j, 2009. 16735

O'Dowd, C. D. and De Leeuw, G.: Marine aerosol production: a review of the current knowledge, *Philos. Trans. R. Soc. A*, 365, 1753–1774, doi:10.1098/rsta.2007.2043, 2007. 16747, 16765

Osborne, S., Johnson, D., Bower, K., and Wood, R.: Modification of the aerosol size distribution within exhaust plumes produced by diesel-powered ships, *J. Geophys. Res.-Atmos.*, 106, 9827–9842, 2001. 16735

Peters, K., Stier, P., Quaas, J., and Graßl, H.: Aerosol indirect effects from shipping emissions: sensitivity studies with the global aerosol-climate model ECHAM-HAM, *Atmos. Chem. Phys.*, 12, 5985–6007, doi:10.5194/acp-12-5985-2012, 2012. 16735

Petters, M. D. and Kreidenweis, S. M.: A single parameter representation of hygroscopic growth and cloud condensation nucleus activity, *Atmos. Chem. Phys.*, 7, 1961–1971, doi:10.5194/acp-7-1961-2007, 2007. 16745

Petzold, A., Hasselbach, J., Lauer, P., Baumann, R., Franke, K., Gurk, C., Schlager, H., and Weingartner, E.: Experimental studies on particle emissions from cruising ship, their characteristic properties, transformation and atmospheric lifetime in the marine boundary layer, *Atmos. Chem. Phys.*, 8, 2387–2403, doi:10.5194/acp-8-2387-2008, 2008. 16735, 16737, 16741, 16746, 16764, 16765

Petzold, A., Weingartner, E., Hasselbach, J., Lauer, P., Kurok, C., and Fleischer, F.: Physical properties, chemical composition and cloud forming potential of particulate emissions from a marine diesel engine at various load conditions, *Environ. Sci. Technol.*, 44, 3800–3805, 2010. 16746, 16764, 16765

Pfaffenberger, L., Baumann, R., Hamburger, T., Weinzierl, B., Schlager, H., and Petzold, A.: The impact of particles emitted from shipping on marine boundary layer aerosol properties and budget, in preparation, 2013. 16737, 16746, 16765, 16767

Porch, W., Borys, R., Durkee, P., Gasparovic, R., Hooper, W., Hindman, E., and Nielsen, K.: Observations of ship tracks from ship-based platforms, *J. Appl. Meteorol.*, 38, 69–81, doi:10.1175/1520-0450(1999)038<0069:OOSTFS>2.0.CO;2, 1999. 16735

Riemer, N., West, M., Zaveri, R. A., and Easter, R. C.: Simulating the evolution of soot mixing state with a particle-resolved aerosol model, *J. Geophys. Res.*, 114, D09202, doi:10.1029/2008JD011073, 2009. 16736, 16741

**Particle-resolved
modeling of a ship
plume**

J. Tian et al.

Title Page

Abstract

Introduction

Conclusions

References

Tables

Figures

◀

▶

◀

▶

Back

Close

Full Screen / Esc

Printer-friendly Version

Interactive Discussion



Russell, L., Seinfeld, J., Flagan, R., Ferek, R., Hegg, D., Hobbs, P., Wobrock, W., Flossmann, A., O'Dowd, C., Nielsen, K., and Durkee, P.: Aerosol dynamics in ship tracks, *J. Geophys. Res.-Atmos.*, 104, 31077–31095, doi:10.1029/1999JD900985, 1999. 16736

Russell, L., Noone, K., Ferek, R., Pockalny, R., Flagan, R., and Seinfeld, J.: Combustion organic aerosol as cloud condensation nuclei in ship tracks, *J. Atmos. Sci.*, 57, 2591–2606, doi:10.1175/1520-0469(2000)057<2591:COAACC>2.0.CO;2, 2000. 16735

Sander, R. and Crutzen, P.: Model study indicating halogen activation and ozone destruction in polluted air masses transported to the sea, *J. Geophys. Res.-Atmos.*, 101, 9121–9138, doi:10.1029/95JD03793, 1996. 16736

Schell, B., Ackermann, I., Hass, H., Binkowski, F., and Ebel, A.: Modeling the formation of secondary organic aerosol within a comprehensive air quality model system, *J. Geophys. Res.-Atmos.*, 106, 28275–28293, doi:10.1029/2001JD000384, 2001. 16742

Shon, Z.-H., Madronich, S., Song, S.-K., Flocke, F. M., Knapp, D. J., Anderson, R. S., Shetter, R. E., Cantrell, C. A., Hall, S. R., and Tie, X.: Characteristics of the NO-NO₂-O₃ system in different chemical regimes during the MIRAGE-Mex field campaign, *Atmos. Chem. Phys.*, 8, 7153–7164, doi:10.5194/acp-8-7153-2008, 2008. 16764

Sinha, P., Hobbs, P., Yokelson, R., Christian, T., Kirchstetter, T., and Bruintjes, R.: Emissions of trace gases and particles from two ships in the southern Atlantic Ocean, *Atmos. Environ.*, 37, 2139–2148, doi:10.1016/S1352-2310(03)00080-3, 2003. 16735

Song, C., Chen, G., and Davis, D.: Chemical evolution and dispersion of ship plumes in the remote marine boundary layer: investigation of sulfur chemistry, *Atmos. Environ.*, 37, 2663–2679, doi:10.1016/S1352-2310(03)00198-5, 2003. 16735, 16736

Twomey, S., Howell, H., Wojciech, T. A., and Conover, J.: Comments on anomalous cloud lines, *J. Atmos. Sci.*, 25, 333–334, doi:10.1175/1520-0469(1968)025<0333:COCL>2.0.CO;2, 1968. 16735

Vogt, R., Crutzen, P., and Sander, R.: A mechanism for halogen release from sea-salt aerosol in the remote marine boundary layer, *Nature*, 383, 327–330, doi:10.1038/383327a0, 1996. 16736

von Glasow, R., Lawrence, M. G., Sander, R., and Crutzen, P. J.: Modeling the chemical effects of ship exhaust in the cloud-free marine boundary layer, *Atmos. Chem. Phys.*, 3, 233–250, doi:10.5194/acp-3-233-2003, 2003. 16736, 16740, 16741

- Winebrake, J. J., Corbett, J. J., Green, E. H., Lauer, A., and Eyring, V.: Mitigating the health impacts of pollution from oceangoing shipping: An assessment of low-sulfur fuel mandates, *Environ. Sci. Technol.*, 43, 4776–4782, doi:10.1021/es803224q, 2009. 16734
- 5 Zaveri, R. and Peters, L.: A new lumped structure photochemical mechanism for large-scale applications, *J. Geophys. Res.-Atmos.*, 104, 30387–30415, 1999. 16741
- Zaveri, R., Easter, R., and Peters, L.: A computationally efficient multicomponent equilibrium solver for aerosols (MESA), *J. Geophys. Res.-Atmos.*, 110, D24203, doi:10.1029/2004JD005618, 2005a. 16741
- 10 Zaveri, R., Easter, R., and Wexler, A.: A new method for multicomponent activity coefficients of electrolytes in aqueous atmospheric aerosols, *J. Geophys. Res.-Atmos.*, 110, D02201, doi:10.1029/2004JD004681, 2005b. 16741
- Zaveri, R. A., Easter, R. C., Fast, J. D., and Peters, L. K.: Model for Simulating Aerosol Interactions and Chemistry (MOSAIC), *J. Geophys. Res.*, 113, D13204, doi:10.1029/2007JD008782, 2008. 16741

**Particle-resolved
modeling of a ship
plume**

J. Tian et al.

Title Page

Abstract

Introduction

Conclusions

References

Tables

Figures

◀

▶

◀

▶

Back

Close

Full Screen / Esc

Printer-friendly Version

Interactive Discussion



**Particle-resolved
modeling of a ship
plume**

J. Tian et al.

Title Page

Abstract

Introduction

Conclusions

References

Tables

Figures

◀

▶

◀

▶

Back

Close

Full Screen / Esc

Printer-friendly Version

Interactive Discussion

**Table 1.** List of hygroscopicity values for model species.

Species	Hygroscopicity, κ
H ₂ SO ₄	0.9
NH ₄ HSO ₄	0.65
NH ₄ NO ₃	0.65
NaCl	1.12
POC	0.001
SOA species	0.1
BC	0.0
Ash	0.1

Particle-resolved modeling of a ship plume

J. Tian et al.

Title Page

Abstract

Introduction

Conclusions

References

Tables

Figures

◀

▶

◀

▶

Back

Close

Full Screen / Esc

Printer-friendly Version

Interactive Discussion



Table 2. Gas phase initial and background conditions.

MOSAIC Species	Symbol	Initial (ppb) ^a	Background (ppb) ^b
Nitric Oxide	NO	8.8×10^5	1.86×10^{-2}
Nitrogen Dioxide	NO ₂	3.7×10^4	3.95×10^{-2}
Nitric Acid	HNO ₃		3.29×10^{-1}
Ozone	O ₃		3.39×10^1
Carbon Monoxide	CO	3.4×10^4	1.05×10^2
Sulfur Dioxide	SO ₂	4.7×10^5	1.55×10^{-1}
Hydrogen Chloride ^c	HCl		5.99×10^{-1}
Paraffin carbon	PAR	3.09×10^5	
Ethene	ETH	2.94×10^4	
Terminal Olefin Carbons	OLET	3.38×10^4	
Internal Olefin Carbons	OLEI	1.55×10^3	
Toluene	TOL	2.56×10^4	
Xylene	XYL	6.06×10^3	

^a Initial data are obtained from HERCULES measurement in 2006 under 75 % engine load condition (Petzold et al., 2008, 2010). The attribution of non-methane hydrocarbons are based on Table 2 in Eyring et al. (2005).

^b Background data are obtained from European program QUANTIFY in 2007. NO_x to NO_y ratio is 0.15 based on Table 2 in Shon et al. (2008) in the marine boundary layer.

^c Value from Table 2 in Keene et al. (2007).

^d If no value is listed the species is initialized with 0 ppb.

Particle-resolved
modeling of a ship
plume

J. Tian et al.

Title Page

Abstract

Introduction

Conclusions

References

Tables

Figures

◀

▶

◀

▶

Back

Close

Full Screen / Esc

Printer-friendly Version

Interactive Discussion

**Table 3.** Aerosol initial, background and ship corridor conditions.^a

Initial	N (m^{-3})	D_g (nm)	σ_g	Composition by Mass (hygroscopicity, κ)
Volatile Mode	2.29×10^{15}	15	1.66	100 % SO_4 (0.9)
Combustion Mode 1	4.36×10^{14}	38	1.40	11.7 % BC + 88.3 % POC (0.0009)
Combustion Mode 2	3.11×10^{10}	155	1.25	27.6 % Ash + 8.4 % BC + 64.0 % POC (0.014)
Background	N (m^{-3})	D_g (nm)	σ_g	Composition by Mass ^b (hygroscopicity, κ)
Aitken Mode	9.6×10^8	40	1.7	9 % SO_4 + 2 % NH_4 + 1 % NO_3 + 82 % POC + 2 % BC + 4 % Sea salt (0.07)
Accumulation Mode	2.3×10^8	200	1.25	22 % SO_4 + 6 % NH_4 + 1 % NO_3 + 64 % POC + 1 % BC + 6 % Sea salt (0.163)
Coarse Mode	3.2×10^6	900	1.8	1 % NO_3 + 5 % POC + 94 % Sea salt (0.999)
Ship corridor	N (m^{-3})	D_g (nm)	σ_g	Composition by Mass
Aitken Mode	7.7×10^{10}	60	1.6	
Accumulation Mode	1.8×10^8	220	1.25	

^a Initial aerosol size distribution and chemical composition data are obtained from HERCULES measurement in 2006 under 75 % engine load condition (Petzold et al., 2008, 2010). Parameters are defined in Eq. (9). Background and ship corridor aerosol size distribution data are obtained from Pfaffenberger et al. (2013). The ship corridor number concentrations represent concentrations above the background level.

^b Background aerosol compositions are estimated from Fig. 5 in O'Dowd and De Leeuw (2007).

Particle-resolved
modeling of a ship
plume

J. Tian et al.

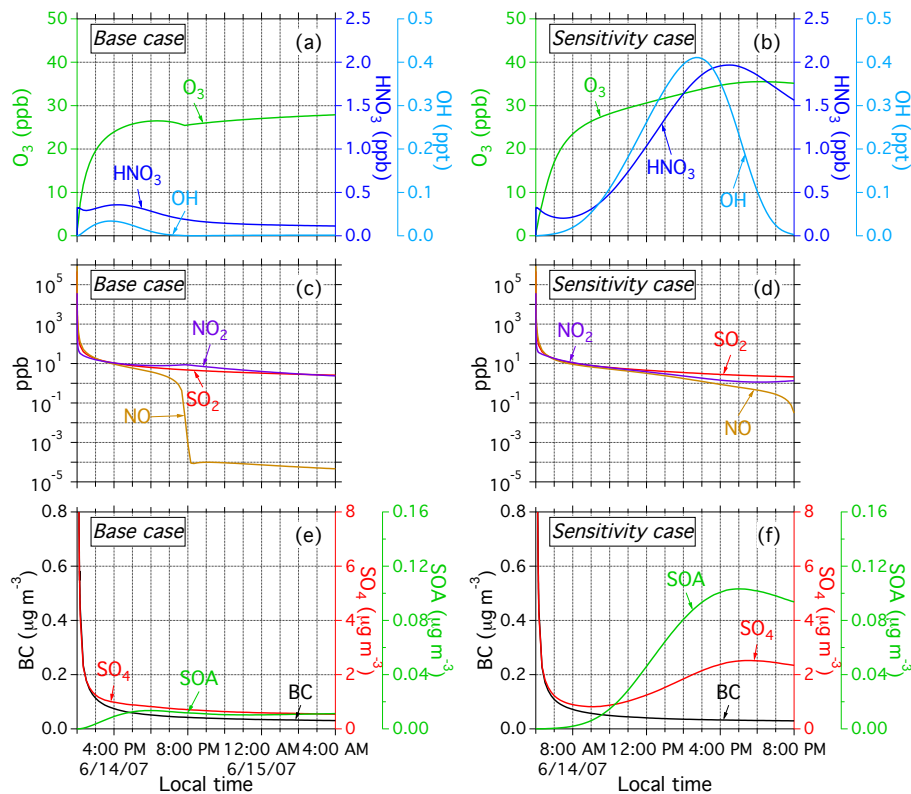


Fig. 1. Evolution of gas and bulk aerosol species in the ship plume over a period of 14 h for the base case starting from 2 p.m. (left column) and sensitivity case starting from 6 a.m. (right column).

Title Page

Abstract

Introduction

Conclusions

References

Tables

Figures

◀

▶

◀

▶

Back

Close

Full Screen / Esc

Printer-friendly Version

Interactive Discussion



Particle-resolved modeling of a ship plume

J. Tian et al.

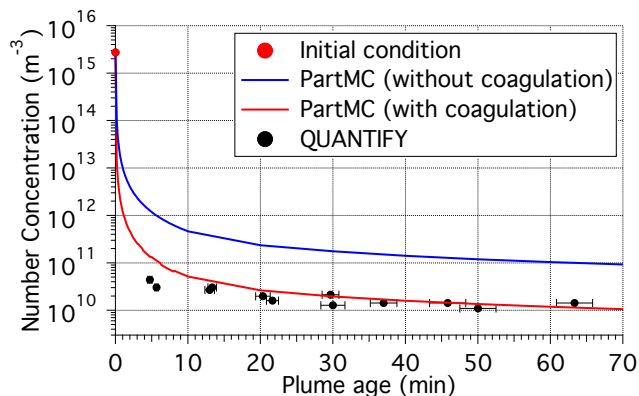


Fig. 2. Comparison of modeled total number concentrations from the base case with the measured data obtained during the single plume study on 14 June 2007 (Pffaffenberger et al., 2013). The red dot indicates the initial aerosol number concentration. The horizontal error bars represent the estimated errors in determining plume ages.

[Title Page](#)[Abstract](#)[Introduction](#)[Conclusions](#)[References](#)[Tables](#)[Figures](#)[◀](#)[▶](#)[◀](#)[▶](#)[Back](#)[Close](#)[Full Screen / Esc](#)[Printer-friendly Version](#)[Interactive Discussion](#)

Particle-resolved modeling of a ship plume

J. Tian et al.

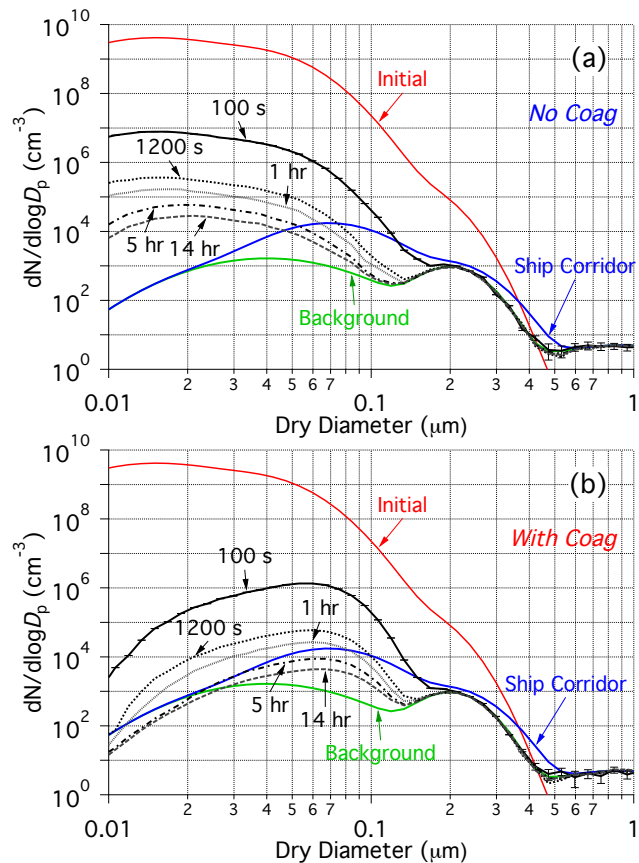


Fig. 3. Measured aerosol number distributions for background, initial and ship corridor and modeled results for **(a)** neglecting coagulation and **(b)** including coagulation at plume ages of 100 s, 1200 s, 1 h, 5 h and 14 h for base case (starting from 2 p.m.). The error bars represent 95% confidence intervals from 10 ensemble runs (only shown for size distribution at 100 s as an example).

Title Page

Abstract

Introduction

Conclusions

References

Tables

Figures

◀

▶

◀

▶

Back

Close

Full Screen / Esc

Printer-friendly Version

Interactive Discussion



Particle-resolved modeling of a ship plume

J. Tian et al.

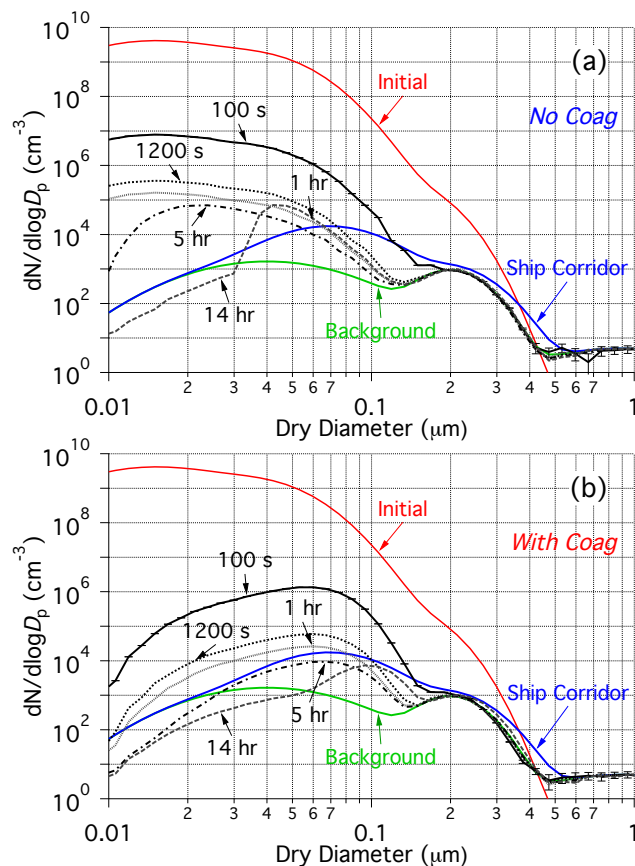


Fig. 4. Measured aerosol number distributions for background, initial and ship corridor and modeled results for (a) neglecting coagulation and (b) including coagulation at plume ages of 100 s, 1200 s, 1 h, 5 h and 14 h for sensitivity case (starting from 6 a.m.). The error bars represent 95 % confidence intervals from 10 ensemble runs (only shown for size distribution at 100 s as an example).

Title Page

Abstract

Introduction

Conclusions

References

Tables

Figures

◀

▶

◀

▶

Back

Close

Full Screen / Esc

Printer-friendly Version

Interactive Discussion



Particle-resolved modeling of a ship plume

J. Tian et al.

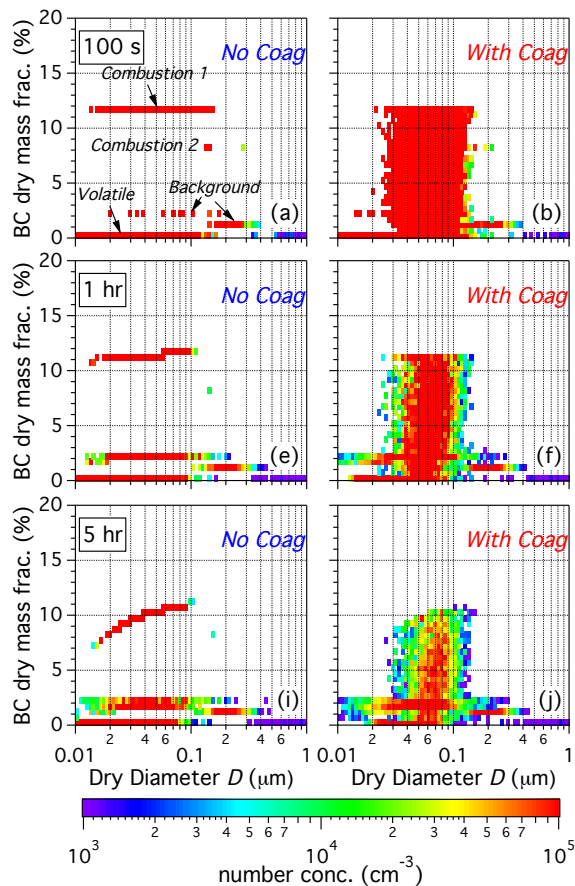


Fig. 5. Two-dimensional number distributions $n_{\text{BC,dry}}(D, w)$ and $n_{\text{SO}_4,\text{dry}}(D, w)$ after 100 s, 1 h and 5 h of simulation for the base case. The two-dimensional number distribution is defined in Eq. (11).

Title Page

Abstract Introduction

Conclusions References

Tables Figures

◀ ▶

◀ ▶

Back Close

Full Screen / Esc

Printer-friendly Version

Interactive Discussion



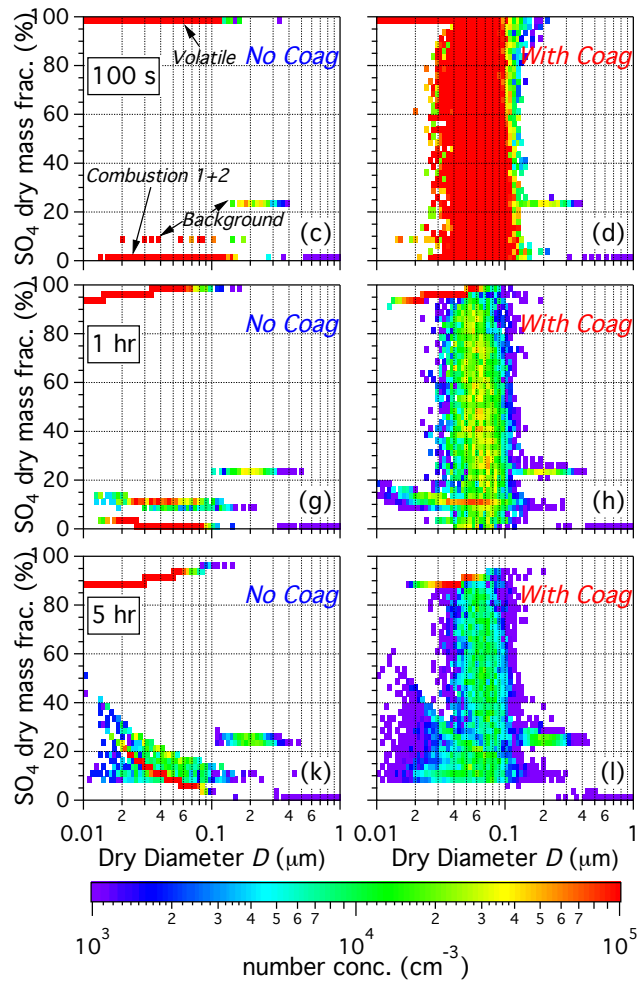


Fig. 5. Continued.

Particle-resolved modeling of a ship plume

J. Tian et al.

Title Page

Abstract Introduction

Conclusions References

Tables Figures

◀ ▶

◀ ▶

Back Close

Full Screen / Esc

Printer-friendly Version

Interactive Discussion



Particle-resolved modeling of a ship plume

J. Tian et al.

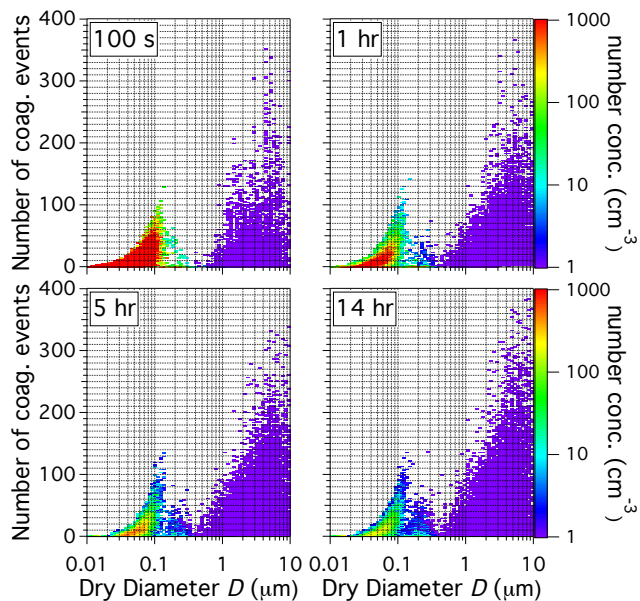


Fig. 6. Two-dimensional number distribution $n_{\text{coag}}(D, k)$ (base case) showing the number of coagulation events experienced after 100 s, 1 h, 5 h and 14 h as defined in Eq. (12).

Title Page

Abstract

Introduction

Conclusions

References

Tables

Figures

◀

▶

◀

▶

Back

Close

Full Screen / Esc

Printer-friendly Version

Interactive Discussion



Particle-resolved modeling of a ship plume

J. Tian et al.

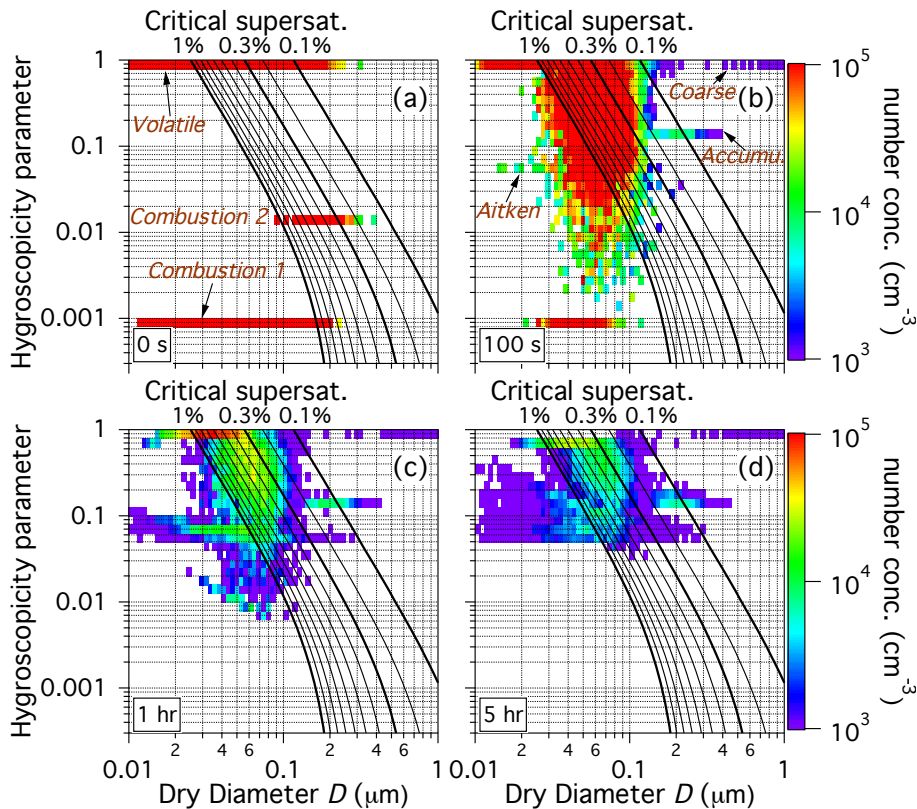


Fig. 7. Two-dimensional number distribution $n_{\kappa}(D, \kappa)$ (base case, coagulation included) at 0 s, 100 s, 1 h and 5 h. The 2-D distribution is defined in Eq. (13).

Title Page

Abstract Introduction

Conclusions References

Tables Figures

◀ ▶

◀ ▶

Back Close

Full Screen / Esc

Printer-friendly Version

Interactive Discussion



Particle-resolved modeling of a ship plume

J. Tian et al.

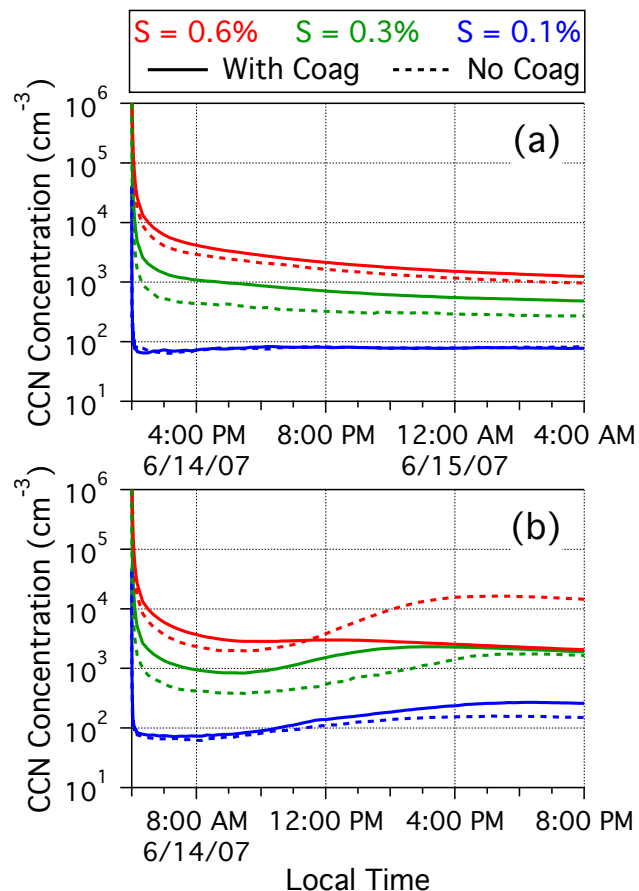


Fig. 8. CCN number concentrations over the entire simulation period for supersaturation thresholds of 0.1% (blue), 0.3% (green) and 0.6% (red) for **(a)** base case, starting from 2 p.m. and **(b)** sensitivity case, starting from 6 a.m. Solid lines are for the simulation including coagulation, dashed lines are for simulations neglecting coagulation.